Energy loss and Z oscillations of atomic beams in plasmas

C. F. Clauser and N. R. Arista
División Colisiones Atómicas, Centro Atómico Bariloche, Instituto Balseiro, 8400 S. C. Bariloche, Argentina
(Received 9 August 2013; published 19 November 2013)

We apply a semiclassical partial-wave-scattering method based on the Wentzel-Kramers-Brillouin approximation to study the transport cross section and the energy loss of neutral or ionized atomic beams in plasmas. This approach reproduces the exact quantum result in a satisfactory manner, even in several extreme conditions of plasma densities and temperatures, and agrees with the results of linear or perturbative calculations for bare ions in the appropriate limits. We pay special attention to low projectile speeds where strong oscillations in the transport cross section and energy loss—as a function of projectile's atomic number—are observed. We study these oscillatory phenomena varying the projectile speed and its ionization degree and the plasma temperature and density. We analyze in physical terms these effects and present a diagram of plasma conditions showing the regions where these oscillations may occur for both neutral and ionized beams.

DOI: 10.1103/PhysRevE.88.053102 PACS number(s): 52.20.Hv, 52.25.Vy, 52.40.Mj, 52.50.Gj

I. INTRODUCTION

The interaction and the ensuing energy loss of neutral or ionized particles in plasmas are problems of central interest for studies on plasma physics. In particular, they are of great interest for current studies on nuclear fusion along the two main research lines: inertial and magnetic confinement, where the interaction with ionized or neutral particles must be considered [1–5].

These two approaches to controlled nuclear fusion are very far in terms of plasma densities and technological aspects. In the first case, inertial confinement fusion (ICF) using either lasers or ion beams, an accurate knowledge of the energy and momentum transfer to small pellets containing the nuclear fuel is required, as well as of the electron and ion transport processes involved. In the second case, magnetic confinement fusion (MCF), neutral beam injection is considered as an important method to deliver energy and momentum to a Tokamak plasma. In addition, the behavior of neutral or ionized impurities in a Tokamak is important to model the behavior and efficiency of the system [6]. Hence, accurate values of transport coefficients and energy transfer between different types of particles and the plasma are a basic requirement for studies concerning both ICF and MCF methods.

Quantitative comparisons between theoretical models and experiments with fusion-plasma targets are rather scarce due to experimental difficulties in producing well-defined conditions for determinations of stopping or transport coefficients through beam-plasma interactions. On the other hand, an accurate knowledge of those coefficients, for different type of ions and plasma conditions, is of great interest for the development of computational codes aiming at describing the effects of impurities and fusion products in the plasma or the injection of neutral or ionized beams. Besides the relevant cases related to the main projects of nuclear energy production previously mentioned, the interactions of ions with dense and dilute plasmas are also of scientific interest for solar and astrophysical studies [7].

Over the years most of the studies of the interaction of ionized particles with plasmas assumed either a pointlike particle or introduced an "effective charge" to represent the test particle, producing in this way a simplification of the problem that eases the theoretical description but does not consider the influence of the internal structure of the particles on the precise magnitude of the interaction coefficients.

Earlier studies of this problem include the cases of dilute and dense media with different theoretical approaches, in particular, collisional [8–10] and dielectric models [11–16].

In the case of cold media, experiments on various solid targets have revealed a strong oscillatory dependence of the stopping coefficients with the projectile atomic number Z_p [17,18], which cannot be described by the theoretical models quoted before. The theoretical description of these effects requires a quantum mechanical approach [19–21] in which the main ingredient is the transport cross section, calculated by means of scattering theory. In a recent work, Mu *et al.* [22] have shown that similar effects may be obtained in the case of plasmas, but the calculations were restricted to neutral atoms, so the effects of projectile ionization were not considered.

In this work, we provide a more extensive study of the conditions in which strong oscillatory effects in the transport and stopping coefficients as a function of Z_p can be expected to occur. Since the results in this case differ so much from those predicted by most commonly used theoretical models, the knowledge of these conditions remains as an important and not yet well-known aspect of ion-plasma interactions, which may have strong influence on the behavior of impurities in fusion plasmas or in ion-plasma experiments using heavy ion beams. The range of applicability of the present study includes the cases of dense conduction electrons in metals, dense and hot plasmas of interest for ICF, and dilute plasmas such as those of interest for MCF, besides several other cases of interest for astrophysical studies. Some of these cases correspond to strongly coupled plasmas [23,24], like in particular the case of solid-state plasmas [19–21,25,26].

The theoretical approach used in this study relies on a recent development of the semiclassical method to treat the problems of electron-ion scattering and energy loss of ions in matter [27]. As will be described in the following, this approach is simple to implement and conserves the accuracy of more sophisticated quantum mechanical methods. Hence, this method is proposed here as a more exact way to describe the interaction of ions and atoms with fusion plasmas.

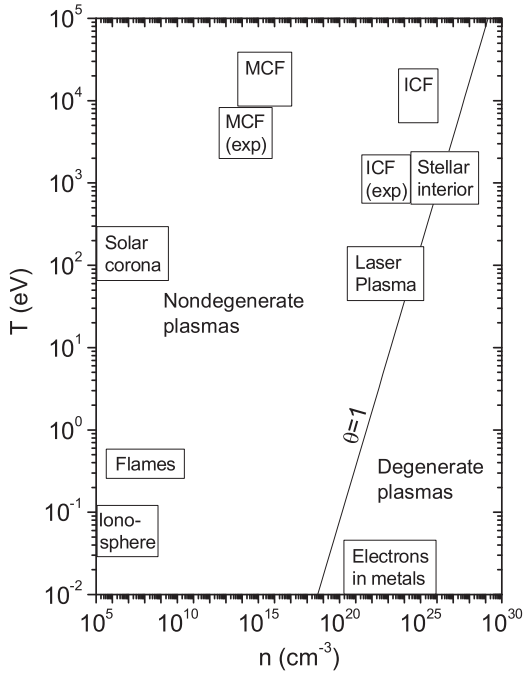

FIG. 1. Schematic diagram of typical plasmas, including cases found in nature or produced in laboratory. MCF refers to magnetic confinement fusion and ICF refers to inertial confinement fusion. The line $\theta = 1$ separates classical (nondegenerate) and quantum (degenerate) plasmas. Here the temperature is given in energy unit, i.e., $T[\text{eV}] = k_B T[\text{K}]$, where k_B is Boltzmann's constant.

A. Plasma parameters

In Fig. 1 we show a scheme of plasma conditions for specific types of plasmas found in nature or produced in the laboratory. The figure includes cases from dilute low-temperature plasmas such as the ionosphere to the opposite extreme of high-density and hot plasmas as required for ICF. The present description is limited to the nonrelativistic range, which corresponds to densities lower than 10^{28} cm^{-3} and electron temperatures below 30 keV. In this work the plasma temperature values are give in eV.

The purpose of this paper is to formulate a method of calculation of the energy loss of neutral or ionized atoms that can be applied on the whole range of plasma conditions illustrated in this figure. The range of applicability of the present approach includes in particular the cases of fusion plasmas with temperatures $T \sim 10^4$ eV (including those of interest for MCF, with densities $n \sim 10^{15}$ cm^{-3}, and ICF, with $n \sim 10^{25}$ cm^{-3}) as well as the stellar interiors, and in the opposite limit, cold plasmas such as those in metals ($n \sim 10^{23}$ cm^{-3}) or the ionosphere ($n \sim 10^5$ cm^{-3}). Therefore, the coverage of the approach allows us to study the transition from highly degenerate (solid-state plasmas) to classical (maxwellian) systems. The range of parameters that characterize these systems are described in Fig. 1. The line $\theta = 1$ in this figure separates the domains where classical ($\theta \gg 1$) or quantum-mechanical ($\theta \ll 1$) descriptions are appropriate. The parameter $\theta = k_B T/E_F$ yields the ratio between thermal and Fermi energies. To carry out this study we describe the electrons in the plasma by the Fermi-Dirac distribution function, considering a homogeneous, isotropic and free of field plasma (see Appendix A).

The neutrality condition of a plasma requires at least two species, so, in principle, we must consider plasma ions and electrons. However, since the ion mass is much larger than the electron mass, the corresponding response time is also much larger. (A simple analysis comparing the relevant response times is given in Appendix B). Because of this condition, the regions where the electronic and ionic contributions to the energy loss are most important are well separated in energy [9]. Since the ionic contribution is fully classical [10], we will restrict this analysis to the electronic stopping term, which is the dominant energy loss channel over a wide range of particle speeds. Moreover, since the electronic and nuclear energy losses are independent processes, an addition of both may be applied in the low-energy range where both could be important.

The paper is organized as follows. In Sec. II we present the semiclassical scheme that we apply to study the problem. In Sec. III we describe the interaction potential and approximations used to cover a wide range of projectile energies and plasma conditions; in Secs. IV to VI we show the results of calculations for several cases of interest, we analyze the results for various plasma and beam-interaction scenarios and we determine the regions where important oscillatory effects appear. Finally, in Sec. VII, we summarize the results and conclusions of this work.

II. THEORETICAL SCHEME: TRANSPORT CROSS SECTION METHOD

As indicated before, our method is based on the semiclassical [Wentzel-Kramers-Brillouin (WKB)] approximation to describe the interaction between the plasma electrons and the external atom or ion through the methods of quantum scattering theory. The central quantity in this description is the transport cross section (TCS), given by [28,29]

$$\sigma_{\text{tr}} = \int (1 - \cos\theta) d\sigma(\theta), \tag{1}$$

which may be written in terms of the scattering phase shifts δ_l as

$$\sigma_{\text{tr}} = \frac{4\pi}{k^2} \sum_l (l+1) \sin^2(\delta_l - \delta_{l+1}). \tag{2}$$

where k is the wave vector corresponding to the scattered electron with relative velocity $v_r = \hbar k/m_e$, with m_e being the electron mass.

To calculate the values of δ_l in an exact way one should solve the Schrödinger equation by numerical methods. However, the number of phase shifts required to obtain a convergent result in most of the cases of interest (Fig. 1) is prohibitively large; for this reason we adopt the semiclassical WKB approach which allows a much faster and usually very accurate solution [27]. In this scheme the phase shifts are calculated by the following

integral [28]:

$$\delta_l = \int dr \sqrt{k^2 - \frac{(l+1/2)^2}{r^2} - \frac{2m_e}{\hbar^2} V(r)} - \int dr \sqrt{k^2 - \frac{(l+1/2)^2}{r^2}}. \quad (3)$$

The integrals go over the range where the corresponding integrand functions are positive. This scheme has been shown to reproduce successfully the exact quantum calculations in a wide range of cases [27]. In the following the present approach will be referred to as the semiclassical partial-wave scattering (SPWS) model.

In particular, perturbative solutions can be obtained using the first-order approximation

$$\delta_l^{\text{pert}} = -\frac{m_e}{\hbar^2} \int_{r_0}^{\infty} \frac{V(r) dr}{\sqrt{k^2 - \left(l + \frac{1}{2}\right)^2 / r^2}}, \quad (4)$$

which yields the perturbative approximation to the transport cross section

$$\sigma_{\text{tr}}^{\text{pert}} \approx \frac{4\pi}{k^2} \sum_l (l+1) \Delta_l^2 \quad (5)$$

with $\Delta_l = \delta_l - \delta_{l+1}$. For instance, for a screened point nucleus with charge $Z_p e$, it can be seen that the Z_p dependence of the transport cross section in the perturbative approximation is simply quadratic. In an improved treatment of close collisions, an additional but weaker Z_p dependence appears in the "collision logarithm" [10]. In particular, this yields the correct Bethe-Bloch limit for bare ions at high energies.

To obtain the stopping power $S \equiv -\langle dE/dx \rangle$ in the scattering theory we must integrate over all relative velocities v_r (between the electrons and the moving ion) and then, over the plasma distribution function, as follows [10]:

$$S(v_p, Z_p) \equiv -\left\langle \frac{dE}{dx} \right\rangle = \frac{\pi m_e n}{v_p^2} \int_0^{\infty} dv_e \, v_e f_{\text{FD}}(v_e) I(v_p, v_e, Z_p) \quad (6)$$

with

$$I(v_p, v_e, Z_p) = \int_{|v_p - v_e|}^{v_p + v_e} dv_r v_r^4 \sigma_{\text{tr}}(v_r, Z_p) \left(1 + \frac{v_p^2 - v_e^2}{v_r^2}\right). \quad (7)$$

Here v_p stands for the projectile speed, v_e represents the electron velocities in the plasma, $f_{\text{FD}}(v_e)$ is the Fermi-Dirac distribution given in the Appendix A, v_r is the relative velocity, given by $v_r = |\mathbf{v}_e - \mathbf{v}_p|$, and n is the electron density.

III. INTERACTION POTENTIALS

Since we are interested in studying the energy loss of atomic projectiles with arbitrary ionization degrees, we describe here the model used for the interaction potential in the various cases of interest. We consider the following cases: (a) bare ions, (b) neutral projectiles, and (c) ions with arbitrary ionization degree.

A. Bare ions

When a static point charge $Z_p e$ is introduced in a plasma, the potential produced by the interaction with plasma electrons is well represented by a Yukawa potential [30,31],

$$V(r) = -\frac{Z_p e}{r} \exp(-r/\lambda_s), \quad (8)$$

where λ_s is the static screening length [32]

$$\lambda_s = \frac{v_s}{\omega_p}, \quad (9)$$

where ω_p is the plasma frequency and v_s is a typical electron speed (see Appendix A).

As discussed in Appendix A, in the limits of low and high temperature the screening length takes the well-known expressions corresponding to Thomas-Fermi and Debye screening, namely $\lambda_{\text{TF}} = v_F/\sqrt{3}\omega_p$ and $\lambda_D = v_{\text{th}}/\omega_p$, respectively. Here v_F refers to the Fermi velocity and $v_{\text{th}} = \sqrt{k_B T/m_e}$ refers to the thermal electron speed.

In the case of swift ions (those moving with velocities much larger than v_s) the screening becomes anisotropic and the range of the screening cloud increases. The effective interaction range in this case is given by the adiabatic screening distance $\lambda_{\text{ad}} = v_p/\omega_p$ and to a good approximation the average interaction may still be described by Eq. (8), where λ_s is replaced by λ_{ad} [32].

The extension of the previous cases to arbitrary (nonrelativistic) projectile speeds may be done using a simple ansatz, which interpolates between the previous limits. In this approach, the model potential for bare ions has the form or Eq. (8), where the dynamical screening length is given by

$$\lambda(v) = \sqrt{\lambda_s^2 + \lambda_{\text{ad}}^2(v)}. \quad (10)$$

This approximation is based on the model description of Ref. [10], where it was shown to yield very good results for the energy loss of bare ions.

While these approximations may be considered appropriate for the case of bare ions, they are not applicable to the more general case of partially ionized or neutral atoms. Hence, we have to introduce a more comprehensive scheme to deal with ionic or neutral projectiles.

B. Neutral atoms

In this case we may approximate the interaction potential by the well-known Molière potential, which provides an accurate fit to the Thomas-Fermi model for atoms. This potential has been widely used to describe the interactions in dense media [33], as well as to calculate the energy loss of atomic projectiles in various conditions [21,34]. The Molière potential is given by

$$V(r) = -\frac{Z_p e}{r} \sum_{j=1}^{3} A_j \exp(-\alpha_j r/a_{\text{TF}}), \quad (11)$$

where $A_j = \{0.1; 0.55; 0.35\}$, $\alpha_j = \{6; 1.2; 0.3\}$, and $a_{\text{TF}} = 0.8853 a_0 Z_p^{-1/3}$ is the Thomas-Fermi radius (where a_0 is the Bohr radius). We can interpret each contribution in the Molière potential, i.e., $j = 1,2$ and 3, as representing an inner, medium, and external screening density, respectively.

C. Arbitrary ionization degree

To extend this study to any degree of projectile ionization, we use the model proposed in Ref. [34] where the ion potential is represented by two terms,

$$V(r) = V_c(r) + V_s(r), \tag{12}$$

where V_c yields the "ion core contribution," which represents the field of the nucleus with the screening provided by its N_e bound electrons, while V_s yields the "external screening" of the ion charge q produced by the plasma electrons.

We define the ionization degree of the projectile by

$$\eta = \frac{q}{Z_p}, \tag{13}$$

where q is the net charge of the projectile and Z_p its atomic number. Then, for a given value of η, we adjust the parameters A_j in the Molière potential ($A_j \to \tilde{A}_j$) and introduce at the same time an external screening component to compensate the ion charge, so we have [34]

$$V(r,v_p) = -\frac{Z_p e}{r}\sum_{j=1}^{3}\tilde{A}_j \exp\{-\alpha_j r\} - \frac{qe}{r}\exp\{-r/\lambda(v_p)\}, \tag{14}$$

where $\sum_j \tilde{A}_j = 1-\eta$ and $\lambda(v)$ is given by Eq. (10). By changing the values of the coefficients $\tilde{A}_j$ in a continuous way, as described in Ref. [34], we can represent ions with arbitrary degrees of ionization. We can note that for $\eta = 0$ ($\tilde{A}_j = A_j$), $V(r,v_p)$ yields the potential of neutral atoms, Eq. (11), while for $\eta = 1$ ($\tilde{A}_j = 0$) we retrieve the case of bare ions, Eq. (8).

IV. TRANSPORT CROSS-SECTION CALCULATIONS

We begin this analysis by showing some examples of quantum mechanical effects in the transport cross section which are beyond the possibility of descriptions based on classical or linear response theories. In the following, atomic units (a.u.) will be used to express some of the results or the calculation parameters.

A first set of calculations is shown in Fig. 2, where we plot the values of the TCS as a function of the ion atomic number for a plasma with density 10^{16} cm^{-3} and temperature of 20 eV for ionization degrees varying from $\eta = 0$ (neutral) to $\eta = 1$ (full ionization). Here we observe a strong oscillatory dependence for neutral atoms, while for the other cases a dependence of the type Z_p^{α} (with $\alpha \sim 1.7$) is obtained. This approaches the Z_p^2 dependence of the perturbative models. In order to show all the curves in the same figure the curves for $\eta = 0$, 0.25, and 0.5 have been multiplied by factors 150, 3, and 2, respectively.

In this case (dilute plasma) the oscillatory behavior is observed only for neutral atoms. However, for dense plasmas, where the screening length becomes much smaller, similar effects can be observed also for ionized projectiles. This is illustrated in Fig. 3 (with density $n = 3.9 \times 10^{23}$ cm^{-3}), where strong oscillations are observed both for neutral and ionized atoms.

This oscillatory phenomenon is a pure quantum effect, produced by the interference of partial waves in Eq. (2). The condition to have large oscillatory effects is that only a few phase shifts with significant values dominate the sum in Eq. (2). Figure 3 shows also a clear change in the behavior when the relative velocity v_r increases, consisting in an attenuation or

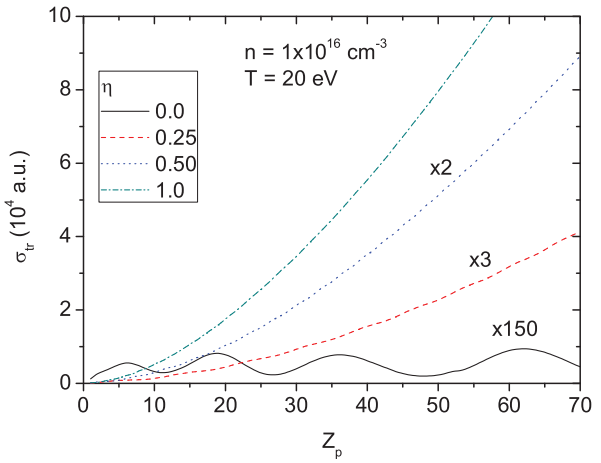

FIG. 2. (Color online) Transport cross section with SPWS model for atomic projectiles interacting with plasma electrons, as a function of atomic number Z_p. The relative velocity here is 1 a.u. The plasma density and temperature are 1×10^{16} cm^{-3} and 20 eV, respectively. The figure shows the disappearance of the oscillatory behavior when the degree of ionization η increases.

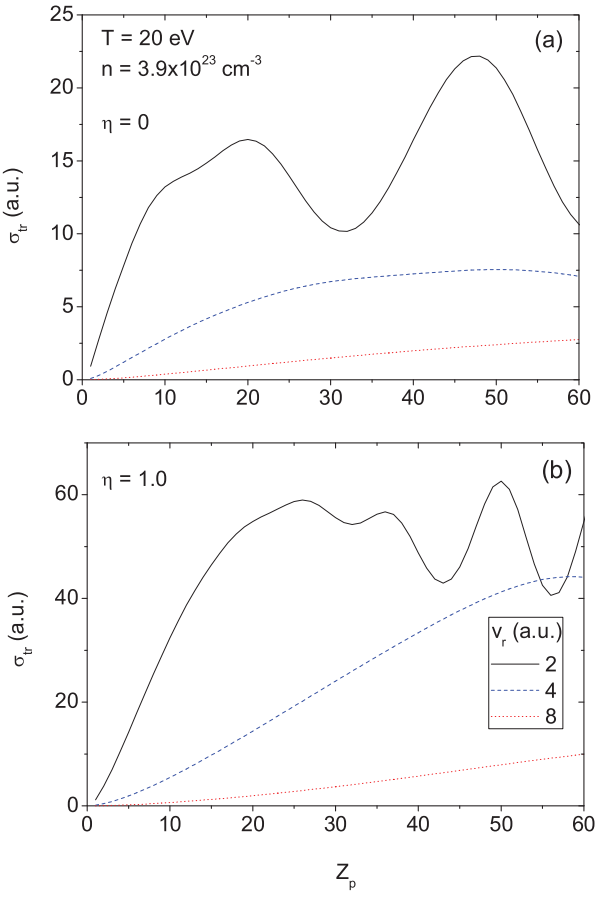

FIG. 3. (Color online) Transport cross section calculated with the SPWS model as a function of atomic number Z_p, for neutral ($\eta = 0$) and bare ($\eta = 1$) ions. The results show the attenuation of the oscillations when the relative velocity v_r increases.

disappearance of the oscillations. It may be shown that for large values of v_r the perturbative approximation works well and in such case the dependence on Z_p becomes a smooth function (in particular, one expects a quadratic dependence on Z_p in first-order perturbation theory, although in these cases we are very far from such behavior).

As we will show later in more detail, the oscillatory effects are more important at low relative velocities and depend on plasma temperature and density, as well as on projectile properties such as its degree of ionization. A more complete analysis will be made in the following sections, where the conditions required to observe these effects will be characterized.

V. ENERGY LOSS CALCULATIONS

We start this set of calculations by showing briefly that the present method is not restricted to low velocities but can be applied in a general way to any velocity in the nonrelativistic range. Figure 4 shows the stopping power of bare ions ($\eta = 1$) with nuclear charges $Z_p = 1$ and 20, calculated from Eq. (6) with the present SPWS model, versus the projectile speed. This figure corresponds to plasma conditions given by $n = 1 \times 10^{18}$ cm^{-3} and $T = 100$ eV.

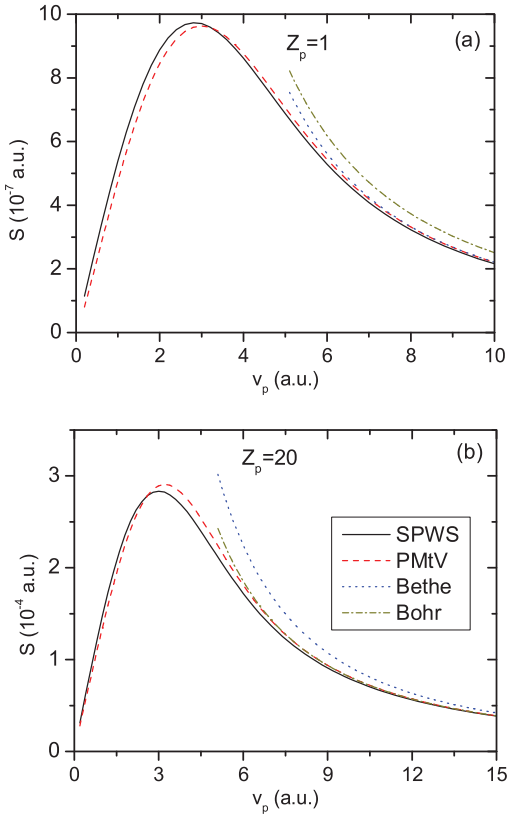

FIG. 4. (Color online) Stopping power as a function of the projectile velocity v_p for two projectile atomic numbers Z_p. In both cases $T = 100$ eV and $n = 1 \times 10^{18}$ cm^{-3}. We compare the SPWS model with a previous dielectric model (PMtV) [16] and with the Bethe and Bohr limits for high energies. In case (a) $Z_p = 1$ and, hence, the Bethe formula gives the correct high-energy limit. In case (b) $Z_p = 20$ and then the correct behavior is given by the Bohr limit.

We compare these results with those obtained from the Peter and Meyer-ter-Vehn'smodel [16] (curves denoted "PMtV"), which was developed for bare projectiles using plasma kinetic theory and dielectric models. In addition, we show in these figures the Bohr and Bethe limits appropriate for high energies.

In Fig. 4(a) the projectile charge is $Z_p = 1$ and, hence, the correct behavior at high speeds is given by the Bethe limit (which applies when $Z_p/v_p < 1$) [35]. On the other hand, Fig. 4(b) corresponds to a higher projectile charge, $Z_p = 20$, and in this case (where $Z_p/v_p > 1$ for the energy range considered) the high-energy behavior agrees with the Bohr limit [35]. In both cases we observe a very good agreement between the semiclassical (SPWS) and the PMtV models and also a good convergence to the corresponding high-energy limits. Notice that when using the PMtV model one must choose the appropriate limit for the cutoff value ($k_{\max}$) in the wave-vector integral, whereas the SPWS model contains it automatically [27].

These examples serve to illustrate the behavior for bare ions and relatively large speeds, where a contact with dielectric or perturbative models is achieved, and we notice also that these models are contained as particular limits of the present description. Since we are interested here in the description of the stronger quantum effects that arise for neutral or ionized beams at intermediate or low energies, where perturbative methods fail, the following discussion will be concentrated on these cases.

VI. QUANTUM OSCILLATIONS IN THE ENERGY LOSS (Z_p OSCILLATIONS)

One of the most interesting features of the energy loss of slow projectiles in matter is the oscillatory dependence on the atomic number Z_p; the discovery of this behavior was a surprising result observed with solid targets [17,18]. More recently, similar effects were predicted for neutral atoms in plasmas [22]. These effects cannot be explained by any of the perturbative or dielectric models [11–16] since it is a typical quantum-mechanical effect.

An explanation of these oscillations was first given by Finneman and Lindhard [19] and studied in more detail by Briggs and Pathak [20,21]. From these works one can see that the oscillations are due to (a) the contribution of few phase shifts usually involved in low-velocity collisional process and (b) the strong dependence of the phase shift values on the projectile atomic number. To explain this in simple terms, we can estimate the maximum value of angular momentum relevant for the scattering of electrons in a screened field,

$$l_{\max} \sim m_e \overline{v_r} \lambda/\hbar, \tag{15}$$

where λ represents the range of the interactions (given, in this case, by the screening length) and $\overline{v_r}$ is a typical value of the relative electron-ion speed. It may be shown that for large values of $l_{\max}$ the interferences between many different partial waves in the sum of Eq. (2) produce a phase-average effect that tends to wash out the oscillations. For this reason, the strongest oscillatory effects are obtained when only few wave components are significant. This effect has been described in previous works for solid targets [19–21].

In fact, in the case of solid targets, one can approximate the stopping power at low velocities ($v_p \ll v_F$) by the expression [19,25]

$$S = nm_e v_p v_F \sigma_{\rm tr}(v_F)$$

and, taking into account that $\sigma_{\rm tr} \sim \sum_l (l+1)\sin^2\Delta_l$, one can expect an oscillatory behavior as a function of Z_p, provided that $l_{\rm max}$ is not large [20,21].

The studies in solids may be taken as limiting cases of calculations for cold and dense systems (solid-state plasmas), and so the question that arises is as follows: What is the behavior of these oscillations when the plasma temperature is increased or the density is decreased? It may be expected that these oscillations will gradually fade away as the conditions of dilute classical plasmas are approached.

In this section we show that the present scheme may be used to cover in a continuous way the transition between the previously described limits of quantum, perturbative, or classical behaviors. In particular, we study the oscillatory effects of the stopping power as a function of the projectile atomic number Z_p, varying the projectile'sspeed and ionization degree and the plasma density and temperature.

A. Z_p oscillations for cold media

As a first test of this approach we consider the interaction of slow ion beams with a carbon target (representing a limit of a cold plasma system) with normal density, $n = 3.9 \times 10^{23}$ cm^{-3}. This is the case where the first evidences of strong oscillatory effects were experimentally obtained [17,18]. In the low velocity range of these experiments (below the Bohr velocity) the electronic energy loss is produced by the excitation of the valence electrons of carbon, which can be represented as a degenerate free electron gas [34].

The results of the present calculations using the SPWS model are shown and compared with experimental data [17,18,36] in Fig. 5. In addition, we show the results of exact quantum scattering theory (obtained by numerical integrations of the Schrodinger equation) [34].

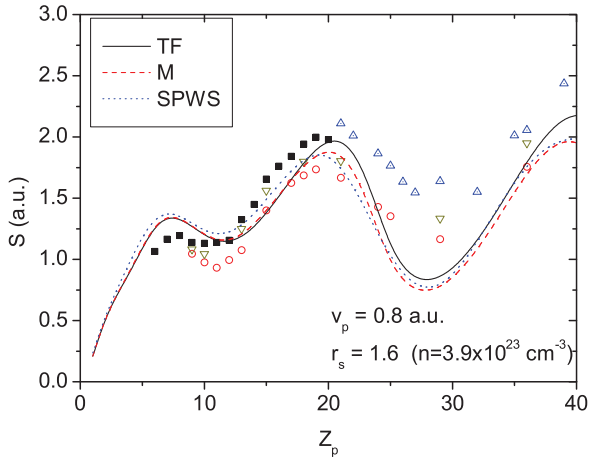

FIG. 5. (Color online) Comparison of stopping power values calculated with the SPWS model, using a Molière potential, with previous quantum mechanical calculations using Thomas-Fermi (TF) and Molière (M) potentials. The experimental values (points) from Refs. [17,18,36] are also shown.

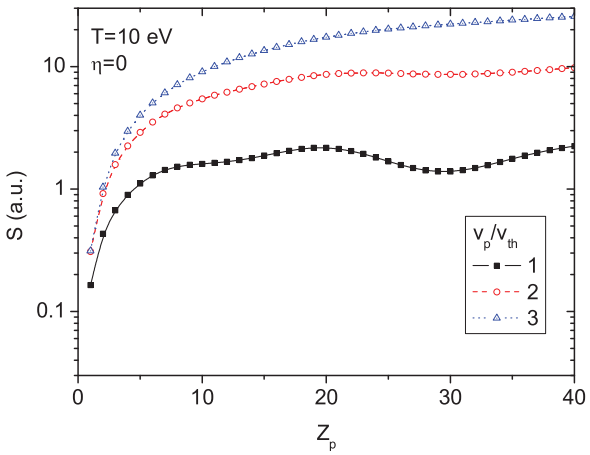

FIG. 6. (Color online) Attenuation of quantum oscillations when the projectile velocity, v_p, increases ($v_p/v_{\rm th} = 1$, 2, and 3). The plasma density is $n = 3.9 \times 10^{23}$ cm^{-3} and $v_{\rm th} = \sqrt{T/m_e}$ is the classical thermal velocity. These calculations correspond to neutral projectiles ($\eta = 0$).

The previous calculations in Ref. [34] were done using both a Thomas-Fermi potential (TF) and a Molière potential (M) to represent the interactions, showing only small differences. The present calculations were made using the Molière potential. We observe a very good agreement of the SPWS model with the exact quantum mechanical results for the same potential. We also find that the present calculations reproduce successfully the oscillations observed in the experimental data, with some discrepancies for Z_p values around 30. The same behavior is observed in the exact results. An explanation of these discrepancies was given earlier by Calera-Rubio *et al.* [37] by considering the effect of inhomogeneities in the electron density of real solids.

B. Attenuation of the Z_p oscillations with increasing v_p

The studies in cold solid targets show that these oscillations are gradually attenuated when the projectile speed increases [34]. We can understand this attenuation considering that when the projectile velocity increases there is a transition from the strong interaction to the perturbative regime. In fact, we observe that the number of phase shifts required for an accurate calculation of the transport cross section increases with ion speed, producing a "mixing" of phase-shift terms in Eq. (2) which gradually attenuates the oscillatory behavior.

This effect is shown in Fig. 6 where we present the results for three ion velocities in a plasma target with the normal carbon density, $n = 3.9 \times 10^{23}$ cm^{-3} and with a temperature $T = 10$ eV (in order to show the three cases in the same figure we use here a logarithmic scale for the energy loss).

C. Attenuation with increasing temperature

Switching now from solids to plasma targets, we can study the changes in the oscillatory phenomenon by varying the plasma temperature. To illustrate these effects we show in Fig. 7 the variation of the stopping power curves with increasing plasma temperature. In these cases the projectile speed is $v_p = 0.5$ a.u.

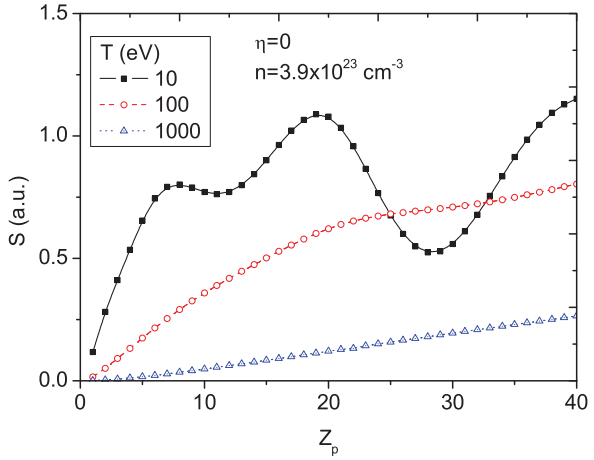

FIG. 7. (Color online) Attenuation of quantum oscillations for slow neutral atoms when the plasma temperature increases ($T = 10$, 100, and 1000 eV). For temperatures larger than 1 keV the Fermi-Dirac function converges to Maxwell-Boltzmann. These calculations correspond to $v_p = 0.5$.

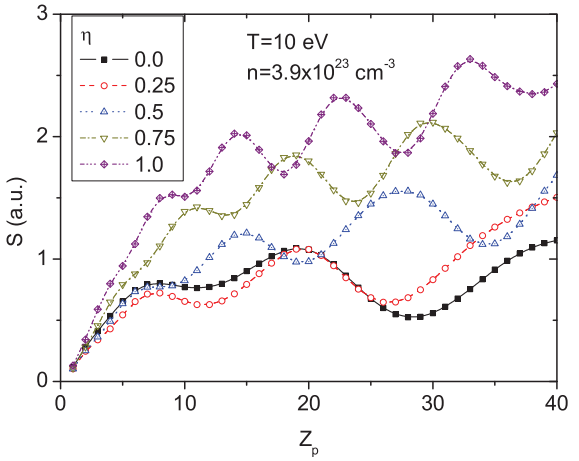

FIG. 8. (Color online) Oscillations of the stopping power for slow ions ($v_p = 0.5$ a.u.) when the ionization degree varies, going from neutral ($\eta = 0$) to bare projectiles ($\eta = 1$). For these plasma conditions ($n = 3.9 \times 10^{23}$ cm^{-3} and $T = 10$ eV) the oscillations occur for any projectile ionization degree.

We note in this figure that the oscillatory behavior disappears when the temperature increases; this effect may be explained by taking into account the dependence of the transport cross section $\sigma_{\rm tr}$ on the relative speed v_r [cf. Eq. (7)] and the sampling of larger electron speeds when the plasma temperature increases.

We note also as an interesting effect the similarity of the stopping curve for $T = 10\ eV$ with those in Fig. 5 for a cold target (although the absolute values are different). It is important to note that the details of the oscillations for neutral ions depend on the projectile's structure; this relation has also been noticed in previous theoretical studies [19,20,22,34]. Here we additionally observe that these oscillations are very sensitive to the projectile speed and to the plasma temperature and that these effects attenuate as a result of a transition from the strong quantum regime to the perturbative regime.

Therefore, the oscillatory behavior of the energy loss as a function of the atomic number is a consequence of (a) the few phase shifts relevant at low speeds and (b) the size and structure of the projectile.

D. Calculations varying the ionization degree

The fact that the oscillations depend on the projectile structure may be illustrated by considering the variation of the stopping curves when the ionization degree η is changed, while maintaining the other parameters fixed. In this case, the plasma screening must be taken into account (in addition to the ion core screening); the range of the screening cloud becomes another important parameter and this confers a different "structure" to the ion.

The effect of the outer screening is to compensate the charge q of the ion by an equal screening charge $-q$. This effect occurs over a distance λ whose value depends on the plasma density and temperature (static screening) and on the ion speed (dynamical screening).

To illustrate this effect, we show in Fig. 8 the changes in the oscillatory pattern when the projectile's ionization degree η varies from 0 (neutral) to 1 (bare ion). For the plasma conditions of this figure ($n = 3.9 \times 10^{23}\,\mathrm{cm}^{-3}$, $T = 10\,\mathrm{eV}$) the oscillatory phenomenon is observed for all ionization states.

However, one can make these oscillations disappear by appropriate changes in the plasma parameters. Quite surprisingly, this effect may be produced in two opposite ways: either by reducing or increasing the density.

A couple of examples are shown in Fig. 9 for chosen densities of (a) $n = 1 \times 10^{21}\,\mathrm{cm}^{-3}$ and (b) $n = 1 \times 10^{25}\,\mathrm{cm}^{-3}$. The temperature in both cases is 10 eV and the projectile speed is $v_p = 0.5$ a.u. It is also surprising to observe here two opposite effects: In the first case one observes oscillations for neutral atoms but not for ionized projectiles, while just the opposite occurs in case (b). We give now an explanation of these seeming paradoxical results.

The explanation stems from the competing roles of two relevant scale lengths: the screening length λ_s (representing the interaction range) and the de Broglie length $\lambda_B = \hbar/m_e v_s$. As is well known from quantum scattering theory, possible interference effects may arise in the interaction of electrons with a screened potential when these two lengths have similar values. These effects disappear when the interaction range λ_s is much larger than the de Broglie length λ_B [notice that this argument is similar to that discussed in connection with Eq. (15)].

In case (a) of Fig. 9, the density of the plasma is relatively low (in an atomic scale) and, hence, the corresponding screening length, for bare ions, is comparatively large ($\lambda_s \sim 14$ a.u. while $\lambda_B \sim 1$ a.u.). Therefore we do not see oscillations in the case of ions. However, if we consider neutral atoms, the plasma screening distance λ_s is no longer relevant and it must be replaced by the atomic screening distance $\lambda_{\rm atom} \sim 1$ a.u. Therefore, for neutral atoms we are in the conditions where $\lambda_B \sim \lambda_{\rm atom}$ and so important oscillations are obtained.

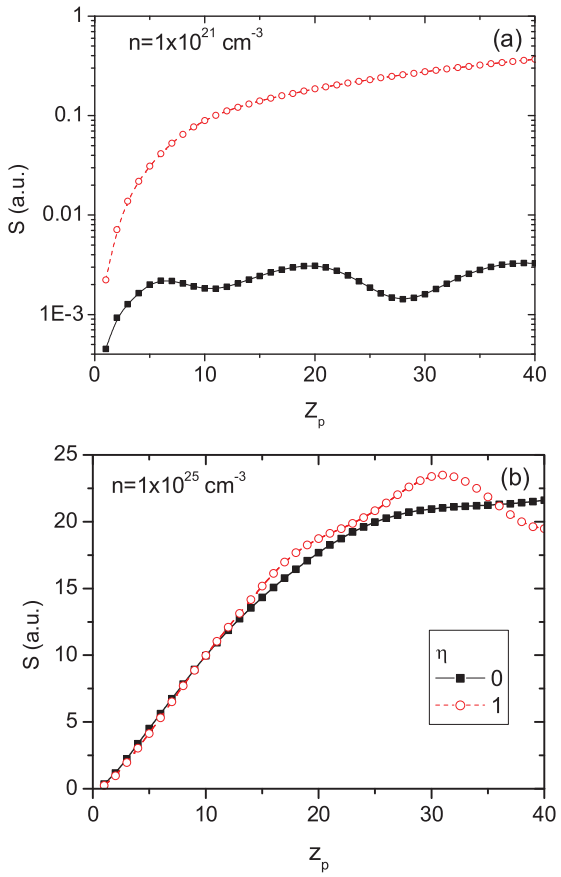

FIG. 9. (Color online) Z_p dependence of the stopping power of slow ions and for two plasma densities. Case (a) shows oscillations for neutral projectiles but not for ionic projectiles. Case (b) shows oscillations for ionic projectiles and not for neutral projectiles. See the text for discussions. In both cases $T = 10$ eV and $v_p = 0.5$ a.u.

In case (b) of Fig. 9, since the density is very high, the Fermi velocity v_F (which yields the typical electron velocity in this case) is also large, and so the de Broglie length becomes smaller ($\lambda_B = \hbar/m_e v_F \sim 0.5$ a.u.). Additionally, because the density is high, the screening distance becomes rather small ($\lambda_s \sim 0.5$ a.u.). Therefore in this case we have a situation where $\lambda_B \sim \lambda_s$, which explains why some oscillations are observed for ions. Instead, in the case of neutral atoms, we find that $\lambda_B < \lambda_{\text{atom}}$ so no oscillations are observed for neutrals.

We may notice, however, that the latter situation of considering neutral atoms in a very high density plasma may not be physically plausible due to the phenomenon of "pressure ionization" which may produce the ionization of the atoms [38].

In the case of low densities, where the Fermi-Dirac distribution converges to the Maxwell-Boltzmann function, the stopping power for neutral projectiles becomes simply proportional to the electron density n; hence, the ratio S/n for neutral atoms becomes independent of n. Figure 10 shows the results for various plasma densities. We can note that, for the whole range where the Maxwell-Boltzmann regime is dominant (up to $n \sim 1 \times 10^{23}$ cm^{-3} in this figure), the curve S/n shows almost no change, while for higher densities a gradual damping of the oscillations is observed.

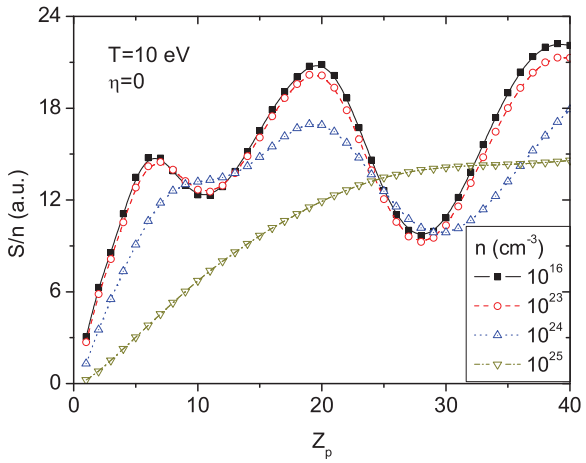

FIG. 10. (Color online) Variation of the Z_p dependence of the stopping power with increasing plasma density for neutral atoms. The curves for densities in the range $n \sim 10^{16}$ cm^{-3} to $n \sim 10^{23}$ cm^{-3} are almost coincident, since the plasma degeneracy is low. The curves for higher densities correspond to partially degenerate plasmas.

E. Summary of cases of interest

To summarize our study of oscillatory phenomena in the transport cross section and energy loss of slow atoms or ions, we show in Fig. 11 a temperature-versus-density diagram, indicating the regions where those oscillations can be expected. As discussed before, for ionic projectiles, the "structure" or size parameter is given by the plasma screening, while for neutral projectiles the corresponding parameter is the atomic size. Therefore, the matching conditions that delimit these regions for ionized and neutral projectiles are

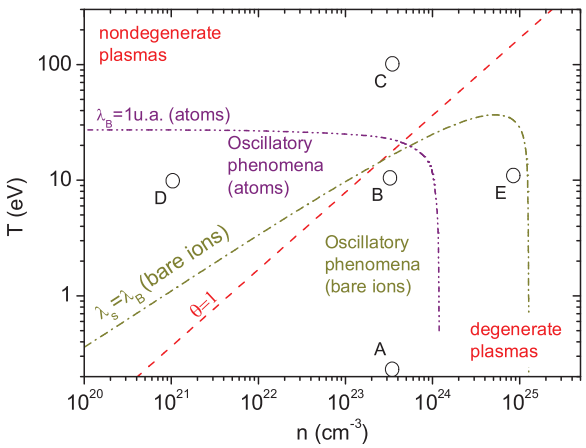

FIG. 11. (Color online) Regions of oscillations diagram for stopping power and transport cross section. The lines show the oscillation conditions for ionic ($\lambda_s = \lambda_B$) and neutral ($\lambda_B \sim 1$ a.u.) projectiles. In both cases we find a high-density limit ($n \sim 1.2 \times 10^{24}$ cm^{-3}, for atoms and $n \sim 1.3 \times 10^{25}$ cm^{-3} for bare ions), where λ_B and λ_s become independent of the plasma temperature (degenerate plasma region). We show with letters A to E some cases studied in this work (Figs. 5 to 10). The $\theta = 1$ line separates the classical and quantum regions.

given by

$$\lambda_B \sim \lambda_s \quad \text{(bare ions)}, \tag{16}$$

$$\lambda_B \sim 1\,\text{a.u.} \quad \text{(neutral atoms)}, \tag{17}$$

where $\lambda_B = \hbar/m_e v_s$ and $\lambda_s = v_s/\omega_p$. These conditions are represented by the dash-dot lines in Fig. 11 and the regions enclosed below these lines are those where important oscillatory effects take place.

The dots marked with letters A to E indicate the particular cases studied in the previous sections. The distribution of dots in this figure serves to explain why we choose such plasma conditions. Since the main oscillation phenomenon takes place at low projectile speeds, we considered only slow particles ($v_p \sim 0$) to produce this diagram.

To further explain the conditions illustrated in Fig. 11 we consider the two limits given by Eqs. (16) and (17) in the following cases:

(i) When $\theta \ll 1$ (i.e., $E_F \gg T$), then $v_s \to v_{\text{TF}}/\sqrt{3}$ (cf. Appendix) and the matching conditions become independent of plasma temperature, giving a high-density limit. In this regime we obtain for neutral projectiles $n \approx 1.2 \times 10^{24}\,\text{cm}^{-3}$, while for bare projectiles we get $n \approx 1.3 \times 10^{25}\,\text{cm}^{-3}$.

(ii) In the classical Maxwell-Boltzmann regime, $\theta \gg 1$ (i.e., $T \gg E_F$), the typical electron speed is $v_s \to v_{\text{th}} = \sqrt{T/m_e}$ (independent of plasma density). Therefore, in this region, in the case of neutral atoms the matching condition yields a temperature limit $T \approx 27$ eV, which is independent of the density. Instead, in the case of bare ions, the relevant screening distance is $\lambda_s \to \lambda_D = v_{\text{th}}/\omega_p$, while $\lambda_B \approx \hbar/m_e v_{\text{th}}$; therefore, the matching condition gives $v_{\text{th}}^2 = \omega_p$ (in a.u.), which yields a straight line with slope $1/2$ in the logarithmic scale. This explains the shape of the curves for atoms and bare ions shown in Fig. 11.

As a case of special interest here, we mention the case of ICF experiments, where a transition from a cold target case to a very hot and dense plasma (i.e., a transition through the points A, B, and C in Fig. 11) occurs.

VII. CONCLUSIONS

We applied the SPWS method to study the interaction of heavy ions with plasmas. Using this approach we explore very different conditions of beam energies and ionization degrees as well as plasma density and degeneracy. The present semiclassical approach reproduces the exact quantum result in a satisfactory manner, even in some extreme cases.

We studied the oscillatory behavior of the energy loss of ion beams (Z_p oscillations) in plasmas for a wide range of plasma conditions. We performed extensive numerical calculations to illustrate the oscillatory phenomenon varying the projectile's ionization degree and its velocity, as well as the plasma density and temperature covering a very wide range of conditions that include the type of plasmas of interest for magnetic- and inertial-confinement fusion research. The oscillatory effects are explained and characterized in terms of the projectile-structure parameters, the screening length, and the de Broglie wavelength associated to plasma electrons. The regions where such oscillatory phenomena may be observed are condensed in a diagram that covers all the cases of interest for the usual laboratory and fusion plasmas, as well as cases of astrophysical interest.

Due to the general character of the method and its extended range of applicability, we propose it as a convenient method to represent in a more accurate way the interaction of atoms and ions with plasmas for a very wide range of conditions.

ACKNOWLEDGMENTS

C.F.C. acknowledges the support from the Consejo Nacional de Investigaciones Científicas y Técnicas (CONICET), Argentina.

APPENDIX A: DISTRIBUTION FUNCTIONS

We summarize here the usual description of the plasma properties in terms of the velocity-distribution function. We consider an isotropic and homogeneous plasma with density n and temperature T in the absence of magnetic fields and with arbitrary degree of degeneracy, so the electrons behave as a free electron gas with a distribution of velocities v corresponding to the Fermi-Dirac statistics, namely

$$f_{\text{FD}}(v) = \frac{C(n,T)}{e^{(\frac{1}{2}m_e v^2 - \mu)/k_B T} + 1}, \tag{A1}$$

where $C(n,T)$ is a normalization coefficient that is determined by the condition

$$\int f_{\text{FD}}(v)\, d^3v = 1. \tag{A2}$$

The chemical potential μ is calculated from the normalization condition as follows [14]. First, we define the degeneracy parameter ζ by

$$\zeta \equiv \theta^{-1} = E_F/k_B T, \tag{A3}$$

where $E_F = m_e v_F^2/2$ is the Fermi energy, with $v_F = \hbar k_F/m_e$ and $k_F = (3\pi^2 n)^{1/3}$. The degeneracy parameter serves to characterize the conditions of classical ($\theta \gg 1$) or quantum ($\theta \ll 1$) behavior of the plasma.

From the normalization condition (A2) we obtain the relation

$$\left[\tfrac{2}{3}F(\mu/k_B T)\right]^{2/3} = \zeta = E_F/k_B T, \tag{A4}$$

where the function $F(s)$ is defined by

$$F(s) = \int_0^\infty \frac{x^{1/2}}{1 + e^{x-s}} dx, \tag{A5}$$

with $s = \mu/k_B T$. These equations determine the chemical potential by $\mu = s k_B T$ as a function of the degeneracy parameter ζ.

The screening of an external point charge in the plasma is given, for arbitrary values of the plasma degeneracy, by the screening length [14]

$$\lambda_s = \frac{v_s}{\omega_p}, \tag{A6}$$

where $\omega_p = (4\pi ne^2/m_e)^{1/2}$ is the plasma frequency and v_s is a particular average of the electronic speed defined by

$$\frac{1}{v_s^2} = \left\langle \frac{1}{v^2} \right\rangle = 4\pi \int_0^\infty f_{\rm FD}(v) dv. \tag{A7}$$

It may be shown that this expression reproduces two well-known limits [14]: For $T \to 0$ we obtain the Thomas-Fermi limit $\lambda_s \to \lambda_{\rm TF} = v_F/\sqrt{3}\omega_p$, whereas for high temperature plasmas ($k_B T \gg E_F$) we retrieve the well-known Debye limit $\lambda_s \to \lambda_D = \sqrt{k_B T/4\pi ne^2}$. These limits correspond to $v_s \simeq v_F/\sqrt{3}$ (degenerate plasma) and $v_s \simeq \sqrt{k_B T/m_e}$ (classical plasma), respectively.

APPENDIX B: RESPONSE TIME

A simplified estimation of the velocity range where the contribution of plasma ions to the total energy loss may be significant can be obtained by considering the response times of the ions and electrons, in relation with the interaction time with moving projectiles. In the following we use subscripts i and e to refer to ions and electrons, respectively.

On one hand, the interaction time of such collisions can be estimated by [39]

$$\Delta t \sim \frac{b}{v_p}, \tag{B1}$$

where b is the impact parameter in the collision between the projectile, with velocity v_p, and the target particle (either electron or ion). The relevant range of impact parameters at low projectile speed is given by the screening length

$$\lambda_{s,e} = v_{{\rm th},e}/\omega_{p,e} \quad \text{(electrons)}, \tag{B2}$$

whereas for the interaction with plasma ions the corresponding value is

$$\lambda_{s,i} = \frac{v_{{\rm th},i}}{\omega_{p,i}} = \frac{1}{Z_i^{1/2}} \frac{v_{{\rm th},e}}{\omega_{p,e}} \quad \text{(ions)}, \tag{B3}$$

where Z_i is the charge of plasma ions (we consider a neutral plasma such that $n = n_e = Z_i n_i$), $v_{{\rm th},e} = \sqrt{T/m_e}$ is the already-defined electron thermal speed and $v_{{\rm th},i} = \sqrt{T/m_i}$ is the corresponding ion speed. $\lambda_{s,i}$ is the ion contribution to the Debye screening length [31].

On the other hand, the response time of each plasma species can be associated to its contribution to the total plasma frequency $\omega_{p,\alpha}$, where α refers to such plasma specie (i.e., either electrons or ions), given by [31]

$$\begin{aligned} \omega_{p,e}^2 &= \frac{4\pi ne^2}{m_e} \\ \omega_{p,i}^2 &= \frac{4\pi n_i (Z_i e)^2}{m_i} = \frac{m_e}{m_i} Z_i \omega_{p,e}^2. \end{aligned} \tag{B4}$$

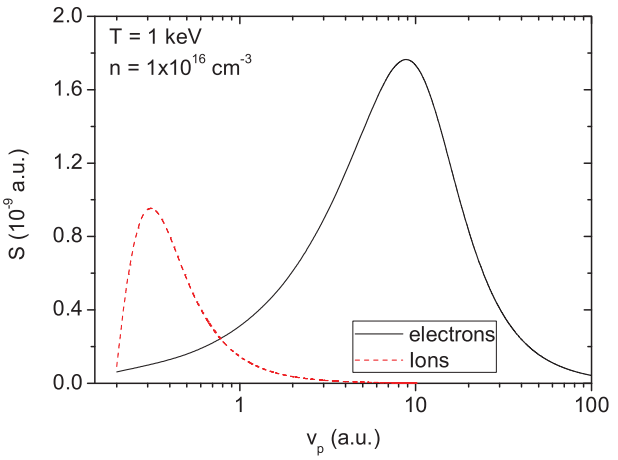

FIG. 12. (Color online) Nuclear and electronic stopping power contributions [10]. We consider a projectile with $Z_p = 1$. The maximum of each curve corresponds to $v_p \simeq v_{{\rm th},i}$ and $v_p \simeq v_{{\rm th},e}$, respectively.

Hence, the relation of times

$$\frac{\lambda_{s,\alpha}}{v_p} \sim \frac{1}{\omega_{p,\alpha}} \tag{B5}$$

gives a condition for which the energy transfer should be important (matching of the interaction time with a typical response time of each species). That is to say, one may expect a significant contribution to the energy transfer when the product $\lambda_{s,\alpha}\omega_{p,\alpha}$ is close to v_p.

It should be noted that the product $\lambda_{s,\alpha}\omega_{p,\alpha}$ yields the corresponding thermal speed, namely

$$\lambda_{s,e}\omega_{p,e} = v_{{\rm th},e}, \tag{B6}$$

$$\lambda_{s,i}\omega_{p,i} = \sqrt{\frac{m_e}{m_i}}\, v_{{\rm th},e} = v_{{\rm th},i}. \tag{B7}$$

Therefore, the criterion here exposed agrees with the so-called Bohr matching condition in the context of atomic excitations [40], which yields an estimation of the velocity at which the corresponding process reaches a maximum, that is, when the projectile velocity matches the orbital speed of the target electrons.

To illustrate this matching condition, we show in Fig. 12 the ionic and electronic contributions to the stopping power for a hydrogen plasma with density $n = 10^{16}{\rm cm}^{-3}$ and temperature $T = 1$ keV, calculated with the de Ferrariis and Arista formulas [10]. Hence, for projectile velocities larger than 1 a.u. the ionic contribution to the stopping power may be neglected.

[1] D. Keefe, Ann. Rev. Nucl. Part. Sci. **32**, 391 (1982).
[2] C. Deutsch, Ann. Phys. Fr. **11**, 1 (1986).
[3] R. C. Arnold and J. Meyer-ter-Vehn, Rep. Prog. Phys. **50**, 559 (1987).
[4] S. Suckewer, H. P. Eubank, R. J. Goldston, J. McEnerney, N. R. Sauthoff, and H. H. Towner, Nucl. Fusion **21**, 1301 (1981).
[5] J. D. Strachan *et al.*, Phys. Rev. Lett. **58**, 1004 (1987).
[6] F. L. Ribe, Rev. Mod. Phys. **47**, 7 (1975).
[7] A. O. Benz, *Plasma Astrophysics: Kinetic Processes in Solar and Stellar Coronae* (Springer, New York, 1993).
[8] M. Gryzinski, Phys. Rev. **107**, 1471 (1957).
[9] S. T. Butler and M. J. Buckingham, Phys. Rev. **126**, 1 (1962).

[10] L. de Ferrariis and N. R. Arista, Phys. Rev. A **29**, 2145 (1984).
[11] J. Lindhard and A. Winther, Mat. Fys. Medd. K. Dan. Vidensk. Selsk. **34**, 4 (1964).
[12] R. H. Ritchie, Phys. Rev. **114**, 644 (1959).
[13] N. R. Arista and W. Brandt, Phys. Rev. A **23**, 1898 (1981).
[14] N. R. Arista and W. Brandt, Phys. Rev. A **29**, 1471 (1984).
[15] G. Maynard and C. Deutsch, Phys. Rev. A **26**, 665 (1982).
[16] T. Peter and J. Meyer-ter-Vehn, Phys. Rev. A **43**, 1998 (1991).
[17] J. H. Ormrod and H. E. Duckworth, Can. J. Phys. **41**, 1424 (1963); J. H. Ormrod, J. R. MacDonald, and H. E. Duckworth, *ibid.* **43**, 275 (1965).
[18] B. Fastrup, P. Hvelplund, and C. A. Sautter, Mat. Fys. Medd. K. Dan. Vidensk. Selsk. **35**, 10 (1966).
[19] J. Finneman, Ph.D. thesis, University of Aarhus, 1968.
[20] J. S. Briggs and A. P. Pathak, J. Phys. C: Solid State Phys. **6**, L153 (1973).
[21] J. S. Briggs and A. P. Pathak, J. Phys. C: Solid State Phys. **7**, 1929 (1974).
[22] Y. Mu, R. Wang, Y. Xia, C. Tan, and L. Mei, Phys. Rev. E **58**, 3777 (1998).
[23] S. Ichimaru, Rev. Mod. Phys. **54**, 1017 (1982).
[24] H. Kitamura and S. Ichimaru, Phys. Rev. E **51**, 6004 (1995).
[25] T. L. Ferrell and R. H. Ritchie, Phys. Rev. B **16**, 115 (1977).
[26] P. M. Echenique, R. M. Nieminen, J. C. Ashley, and R. H. Ritchie, Phys. Rev. A **33**, 897 (1986).
[27] N. R. Arista and P. Sigmund, Phys. Rev. A **76**, 062902 (2007).
[28] L. D. Landau and E. M. Lifshitz, *Quantum Mechanics: Non-Relativistic Theory* (Pergamon Press, Oxford, 1960).
[29] N. F. Mott and H. S. W. Massey, *The Theory of Atomic Collisions*, (Oxford University Press, Oxford, 1950).
[30] N. A. Krall and A. W. Trivelpiece, *Principles of Plasma Physics* (McGraw-Hill, New York, 1973).
[31] S. Ichimaru, *Basic Principles of Plasma Physics* (Benjamin, Reading, MA, 1973).
[32] J. Neufeld and R. H. Ritchie, Phys. Rev. **98**, 1632 (1955).
[33] F. F. Komarov, *Energy Loss and Ion Ranges in Solids* (Gordon & Breach, New York, 1981).
[34] N. R. Arista, Nucl. Instrum. Methods Phys. Res. B **195**, 91 (2002).
[35] P. Sigmund, *Particle Penetration and Radiation Effects* (Springer, New York, 2005).
[36] W. N. Lennard, H. Geissel, D. P. Jackson, and D. Phillips, Nucl. Instrum. Methods Phys. Res. B **13**, 127 (1986).
[37] J. Calera-Rubio, A. Gras-Marti, and N. R. Arista, Nucl. Instrum. Methods Phys. Res. B **93**, 137 (1994).
[38] R. M. More, Adv. At. Mol. Phys. **21**, 305 (1985).
[39] J. D. Jackson, *Classical Electrodynamics* (Wiley, New York, 1975).
[40] N. Bohr, Mat. Fys. Medd. K. Dan. Vidensk. Selsk. **18/8**, 1 (1948).